

# Method for Generating High Purity Laguerre-Gaussian Vortex Modes

Robin Uren, Stephen Beecher, Callum R. Smith, W. Andrew Clarkson

**Abstract**—Generation of a donut-shaped first-order Laguerre-Gaussian ( $LG_{01}$ ) vortex mode via a method designed to yield high mode purity is reported. Our approach utilises a novel twin-spot end-pumping scheme to directly excite the first order Hermite-Gaussian ( $HG_{01}$ ) mode in a solid-state laser, followed by a novel astigmatic mode converter based on spherical (concave) mirrors aligned at oblique incidence. A simple theoretical model for the mode converter is derived and from this the design approach is explained along with the potential benefits compared to conventional schemes based cylindrical-lens astigmatic mode converters, particularly for power scaling. As a proof-of-principle and to confirm the benefits of this scheme in terms of high mode purity we have applied it to an end-pumped Nd:YVO<sub>4</sub> laser to generate a ( $LG_{01}$ ) beam with a controllable sense of azimuthal phase and hence orbital angular momentum. A method for characterising the resulting beam based on analysis of the spiral interference pattern derived with the aid of a Mach-Zehnder interferometer is described and yields a value for the  $LG_{01}$  mode purity of 94%. Common sources of mode impurity are identified and the prospects for scaling to higher power whilst maintaining high mode purity are considered.

**Index Terms**—Laser Modes, Solid Lasers

## I. INTRODUCTION

THERE has been considerable interest in vortex modes as their unique properties give them wide ranging applications. Key areas of interest include atom trapping, optical communications, sub-wavelength microscopy and laser processing [1], [2]. Vortex modes are a subset of Laguerre-Gaussian ( $LG$ ) cavity modes that have a helical phase structure. This is the source of the mode's orbital angular momentum (OAM). Our primary interest is in the area of laser processing of materials, which has attracted considerable attention due to some early experiments demonstrating the production of chiral structures [3] and higher quality laser ablation [4], [5]. However, so far most demonstrations of machining with vortex modes have been limited by the beam quality achievable at high average powers and pulse energies [1], [3], [4]. It is therefore difficult to ascertain with confidence the effect of the OAM on the machining process. This suggests there is a need for a more robust, power scalable technique for generating highly pure vortex modes. It is also essential that this technique be accompanied by a suitable diagnostic capability for determining mode purity. The  $M^2$  parameter, which is a good indicator of the purity of Gaussian fundamental transverse ( $TEM_{00}$  or  $HG_{00}$ ) mode beams, is not sufficient for higher order modes. Quantifying the quality of these modes therefore requires more careful analysis.

There are several popular methods for generating the first order Laguerre-Gaussian ( $LG_{01}$ ) vortex mode. Direct generation internally within a laser cavity has the potential to yield a very high purity vortex mode. However, in practice, this is rather challenging due to the fact that there are a number of modes with identical transverse intensity distributions including,  $LG_{01}^+$  modes with clockwise (CW) handedness and  $LG_{01}^-$  modes with counter-clockwise (CCW) handedness, radially-polarized and azimuthally-polarized modes that do not carry OAM and incoherent combinations of orthogonally orientated ( $HG_{01}$ ) modes [6]. This makes preferential selection of the desired mode (i.e.  $LG_{01}^+$  or  $LG_{01}^-$ ), whilst at the same time suppressing unwanted modes extremely difficult. Clearly, a prerequisite for achieving this is a means for discriminating between vortex modes with opposite handedness. The use of annular shaped pump beams [7], [8], [9] or spot defect mirrors [10], [11] to create matching gain or loss distributions to the desired mode have been employed for direct generation of donut modes, but, for the reasons stated above, cannot guarantee robust operation on a high purity vortex mode. In addition to the use of an annular pump beam, Di Lin *et al.* in [12] exploit the different intracavity standing-wave intensity distributions for  $LG_{01}^+$  and  $LG_{01}^-$  vortex modes in a standing-wave laser using two nano-wires inserted into the cavity to differentiate between these modes by virtue of creating a differential loss. This approach, however, has the shortcoming that the nano-wires have to be aligned to subwavelength accuracy to generate the desired mode making practical implementation difficult.

Alternatively, vortex modes can be generated external to the laser using, for example, a spiral phase plate [13], [14] or a liquid crystal spatial light modulator [15] to convert a fundamental laser ( $HG_{00}$ ) mode into a  $LG_{01}^\pm$  mode. These schemes have the attraction of being straightforward to implement, but as they only impart an azimuthal phase variation on to the fundamental mode, they have the shortcoming that they do not yield a very pure vortex mode. Moreover, spatial light modulators have rather limited power handling and hence are not suitable for the high powers generally required for applications in laser processing.

Another approach for producing a vortex mode is to employ an astigmatic mode converter (AMC). This approach was initially proposed by C. Tamm and C. Weiss [16] and later expanded upon by M.W. Beijersbergen *et al.* in [17]. The AMC, as conceived in [17], comprises two cylindrical lenses aligned parallel and with respect to an incident beam so to yield an astigmatic region between the lenses. In this way, the the Gouy phase shift between orthogonal beam components at 45° to the lens axes over the astigmatic region can be manipulated to allow a high-order Hermite-Gaussian ( $HG$ ) beam to be converted into a

Manuscript received March ??, 2019; revised ??, 2019. (Corresponding author: W. Andrew Clarkson.) The authors are with the Optoelectronics Research Centre, University of Southampton, Southampton, SO17 1BJ, UK. (email: wac@orc.soton.ac.uk).

Laguerre-Gaussian (*LG*) beam or vice versa. The AMC is a popular method for converting a  $HG_{01}$  mode into a  $LG_{01}$  vortex mode and has been shown theoretically capable of producing vortex modes of very high purity [18]. However, this requires high quality cylindrical lenses, precise alignment and a high quality  $HG$  mode. These conditions are not straightforward to satisfy as cylindrical lenses tend to be of poorer quality than spherical optics. Moreover, standard methods for producing  $HG_{01}$  modes (e.g. by pump beam offset and mirror misalignment) tend to yield beams with significant mode impurities.

In this paper, we describe a method for generating high purity  $LG_{01}$  vortex modes that employs a new design of AMC based on spherical mirrors aligned at oblique incidence in combination with a twin-spot end-pumping scheme to generate a high quality  $HG_{01}$  mode. This approach has been applied to an end-pumped Nd:YVO<sub>4</sub> laser and we explore both theoretically and experimentally the impact of misalignment on  $LG_{01}$  mode purity. Through careful optimisation of the AMC design and alignment we demonstrate an  $LG_{01}$  mode purity of >94% and consider measures that could yield a further improvement in mode purity. Finally, we consider merits of our scheme for the generation of high power vortex beams for applications such as laser processing of materials.

## II. THEORY

We begin by developing the theory for the AMC based on spherical mirrors in order to understand the design criteria, following the approach developed by M.W. Beijersbergen *et. al.* in [17] for the cylindrical lens AMC. The electric field for a  $HG$  mode may be expressed in Cartesian coordinates  $x$ ,  $y$  and  $z$  as

$$E_{HG}(x, y, z) = E_0 \frac{w_0}{w(z)} H_m \left( \frac{\sqrt{2}x}{w(z)} \right) H_n \left( \frac{\sqrt{2}y}{w(z)} \right) \exp \left( \frac{-(x^2 + y^2)}{w(z)^2} \right) \exp \left( \frac{i\pi(x^2 + y^2)}{2\lambda R(z)} \right) \exp \left( \frac{-i2\pi z}{\lambda} \right) \exp(i(m+n+1)\zeta(z)) \quad (1)$$

where  $E_0$  is a scaling factor,  $w_0$  is the beam radius of the fundamental ( $HG_{00}$ ) mode at the waist position,  $x, y$  are transverse positions,  $z$  is the position along the propagation direction from the waist,  $w(z)$  is the beam radius at distance  $z$  from the waist position,  $m$  and  $n$  are the mode orders in  $x$  and  $y$  directions respectively,  $H_m$  is the Hermite polynomial of order  $m$ ,  $\lambda$  is the wavelength,  $R(z)$  is the radius of curvature of the wavefront at distance  $z$ ,  $\zeta(z)$  is the Gouy phase shift and  $z_R$  is the Rayleigh range given by

$$z_R = \frac{\pi w_0^2}{\lambda} \quad (2)$$

The beam radius,  $w(z)$  and Gouy phase,  $\zeta(z)$  evolve with propagation distance,  $z$ , according to

$$w(z) = w_0 \sqrt{1 + \left( \frac{z}{z_R} \right)^2} \quad (3)$$

$$\zeta(z) = \arctan \left( \frac{z}{z_R} \right) \quad (4)$$

Physically the Gouy phase shift represents the phase change, relative to a plane wave, that a transverse mode experiences as it passes through a focus [19]. For a higher order ( $HG_{m,n}$ ) mode and non-astigmatic focusing, the total Gouy phase,  $\Psi(z)$ , evolves with distance from the beam waist according to

$$\Psi(z) = (m+n+1)\zeta \quad (5)$$

However, for astigmatic focusing with the beam waist in the sagittal plane ( $y, z$ ) sharing the same position (i.e. at  $z=0$ ) with the beam waist in the tangential plane ( $x, z$ ) equation (5) should be modified to

$$\Psi(z) = (m+1/2)\zeta_S + (n+1/2)\zeta_T \quad (6)$$

to take into account the different values for the Rayleigh range,  $z_{RS}$  and  $z_{RT}$ , and hence the different Gouy phase shifts,  $\zeta_S$  and  $\zeta_T$ , in the sagittal ( $S$ ) and tangential ( $T$ ) planes respectively. The principles of operation of the spherical mirror AMC for the purpose of converting a  $HG_{01}$  mode to an  $LG_{01}$  vortex mode are illustrated in Fig. 1 and Fig. 2. A  $HG_{01}$  beam with its lobes orientated

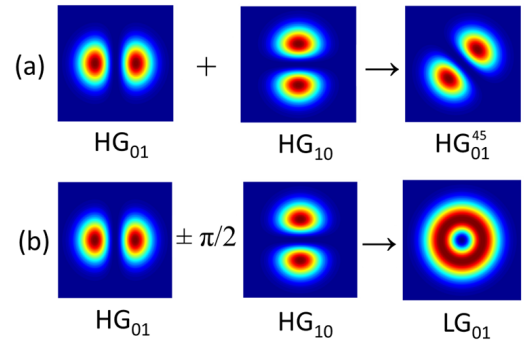


Fig. 1: (a) Schematic showing that a  $HG_{01}$  mode orientated at  $45^\circ$  is equivalent to a coherent combination of  $HG_{01}$  and  $HG_{10}$  modes. (b) Schematic showing that a  $LG_{01}$  vortex mode is equivalent to a coherent combination of  $HG_{01}$  and  $HG_{10}$  modes with a phase difference of  $\pi/2$ .

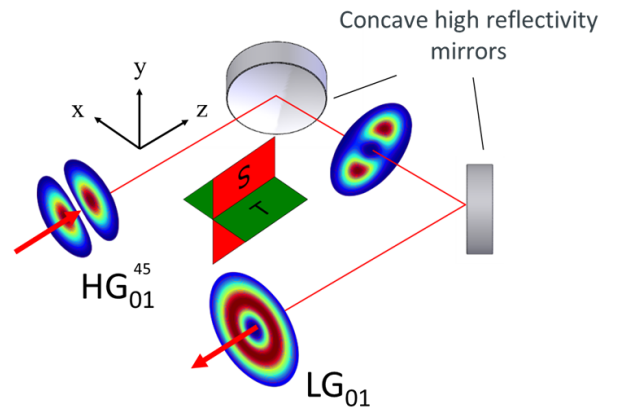


Fig. 2: Diagram of an AMC based on spherical mirrors. Both the coordinate axes and the sagittal,  $S$ , and tangential,  $T$ , planes are defined as they are used throughout this paper.

at  $45^\circ$  to the  $S$  and  $T$  planes, labelled for convenience as a  $HG_{01}^{45}$  mode, is incident on the spherical mirror astigmatic mode converter as shown. This beam can be considered as a coherent superposition of  $HG_{01}$  and  $HG_{10}$  modes as illustrated in Fig. 1(a). The spherical mirror mode converter simply comprises two very high reflectivity concave mirrors of equal radius of curvature separated by a distance  $(2d)$  and aligned so that the beam strikes both at the same angle of incidence (see Fig. 2). The incident beam parameters (i.e. beam waist size and position) are selected so that a beam waist is formed at the mid-point ( $z = 0$ ) of the arm between the two concave mirrors (i.e. at a distance  $d$  from each mirror). The combined  $HG_{01}$  and  $HG_{10}$  beam form different size beam waists,  $w_{0S}$  and  $w_{0T}$ , in the astigmatic region between the two concave mirrors due to the different focal lengths for the mirrors in the  $S$  and  $T$  planes that result from the oblique angle of incidence of the beams (see Fig. 3). As a result of the symmetrical

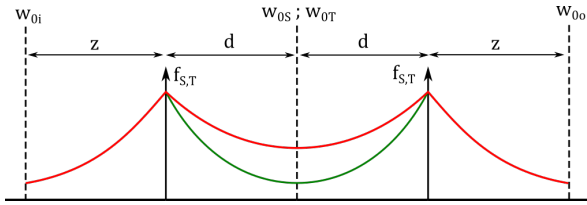


Fig. 3: Schematic showing the evolution of beam radii in the sagittal (red line) and tangential (green line) planes with distance within the spherical mirror AMC. The beam radii in the sagittal and tangential planes are equal before and after the AMC and evolve with distance as shown by the red line.

nature of the AMC, the  $HG_{01}$  and  $HG_{10}$  beams exiting the final AMC mirror have the same beam parameters (i.e. beam radius and wavefront curvature) as at the input mirror. In the astigmatic region between the two mirrors, the Gouy phase shifts,  $\Psi_{10}$  and  $\Psi_{01}$ , for the respective  $HG_{01}$  and  $HG_{10}$  components evolve differently with the result that there is a net phase shift,  $\Delta\Psi$ , between the beams as they exit the final AMC mirror given by

$$\begin{aligned} \Delta\Psi &= \Psi_{01} - \Psi_{10} = \zeta_T - \zeta_S \\ &= 2 \arctan\left(\frac{d}{z_{RT}}\right) - 2 \arctan\left(\frac{d}{z_{RS}}\right) \end{aligned} \quad (7)$$

where  $d$  is the distance from the beam waist to AMC input (or output) mirror. From (7) it can be seen that  $\Delta\Psi$  depends only on the Rayleigh ranges,  $z_{RT}$  and  $z_{RS}$ , for the beam in the astigmatic region and on the separation of the mirrors. In Fig. 1(b) it is shown that an  $LG_{01}$  vortex mode is a coherent superposition of  $HG_{01}$  and  $HG_{10}$  modes with a  $\pi/2$  phase difference. Thus, by arranging for  $\Delta\Psi = \pi/2$  in (7) we can convert the incident  $HG_{01}^{45}$  mode into a  $LG_{01}$  vortex mode. Further simplification of (7) reveals that this condition is satisfied when

$$z_{RT} = d \left( \frac{z_{RS} - d}{z_{RS} + d} \right) \quad (8)$$

In order for the beam to be stigmatic outside the AMC, the beam radii in orthogonal  $S$  and  $T$  planes at the entrance and exit to the AMC (i.e. at  $z = \pm d$ ) must be equal.

From (2) and (3) we see that this yields the following relationship between  $z_{RT}$ ,  $z_{RS}$  and  $d$ :

$$\frac{z_{RT}^2 + d^2}{z_{RT}} = \frac{z_{RS}^2 + d^2}{z_{RS}}, \quad (9)$$

which can be further simplified to

$$z_{RS}z_{RT} = d^2 \quad (10)$$

From equations (8) and (10) we can then obtain the following expressions for  $z_{RT}$  and  $z_{RS}$

$$z_{RT} = d \left( \sqrt{2} - 1 \right) \quad (11)$$

$$z_{RS} = d \left( \sqrt{2} + 1 \right) \quad (12)$$

We can now apply one final boundary condition, namely, that the radii of curvature of the wavefronts for the beam incident and emerging from the AMC must be equal in both the  $S$  and  $T$  planes. This leads to the following relation between the radii of curvature of the wavefronts,  $R_S$  and  $R_T$ , of the beam in the astigmatic region of the AMC immediately adjacent to the concave mirrors in the  $S$  and  $T$  planes, respectively.

$$\frac{1}{R_i} = \frac{1}{R_S} - \frac{1}{f_S} = \frac{1}{R_T} - \frac{1}{f_T} \quad (13)$$

where  $R_i$  is the radius of curvature of the beam incident on the AMC, and  $f_S$  and  $f_T$  are the focal lengths of the concave mirrors in the  $S$  and  $T$  planes, respectively. The above expression can be re-written as follows:

$$\Delta D = \frac{1}{f_T} - \frac{1}{f_S} = \frac{1}{R_T} - \frac{1}{R_S} \quad (14)$$

where  $\Delta D$  is the difference in dioptric power for the concave mirrors in the  $S$  and  $T$  planes.  $R_S$  and  $R_T$  are related to the respective Rayleigh ranges,  $z_{RT}$  and  $z_{RS}$ , by [20]

$$R_S = \frac{d^2 + z_{RS}^2}{d} \quad (15)$$

$$R_T = \frac{d^2 + z_{RT}^2}{d} \quad (16)$$

Substituting (11) and (12) into (15) and (16) and then the resulting expressions into (14) yields the following simple expression relating  $d$  to  $\Delta D$ :

$$d = \frac{1}{\Delta D \sqrt{2}} \quad (17)$$

It is worth noting that the above relation also applies to the more general case where custom-shaped lenses (or mirrors) with different focal lengths in orthogonal planes are used, as well as for the situation of interest here where the difference in focal lengths in orthogonal planes is derived by employing standard concave high reflectivity mirrors at an oblique angle of incidence. For the case of a cylindrical lens AMC with a focal length,  $f$ , (17) reduces to  $d = f/\sqrt{2}$  in agreement with the analysis described by M.W. Beijersbergen *et al.* in [17]. For an AMC based on concave mirrors aligned with respect to the beam at an angle-of-incidence,  $\theta$ , the focal lengths in  $S$  and  $T$  planes can be written as [21]

$$f_S = \frac{R_c}{2 \cos(\theta)} \quad (18)$$

$$f_T = \frac{R_c \cos(\theta)}{2} \quad (19)$$

where  $R_c$  is the radius of curvature of the concave mirrors. Substituting (18) and (19) into (14) yields the following expression relating  $d$  to the mirror parameters:

$$d = \frac{R_c}{2\sqrt{2} \sin(\theta) \tan(\theta)} \quad (20)$$

It can be seen from (20) that the design of a spherical mirror AMC is very straightforward given the availability of suitable concave mirrors with high reflectivity dielectric coatings at the desired angle of incidence. One practical point worth mentioning is that relatively large angles of incidence are needed to avoid an excessively long mirror separation. Whilst the design of the AMC is simple, it is crucial that the incident  $HG_{01}^{45}$  beam has high purity and has the correct size and wavefront curvature for the chosen AMC design. Substituting (11) or (12) into (3) yields the following expression for the incident beam radius in both the  $S$  and  $T$  planes:

$$w(d) = \left( \frac{2\sqrt{2}\lambda d}{\pi} \right)^{1/2} \quad (21)$$

Similarly, the following expression for the radius of curvature,  $R_i$ , of the beam incident on the AMC can be obtained by substituting (12) and (15) into (13):

$$\frac{1}{R_i} = \frac{1}{2d(2 + \sqrt{2})} - \frac{1}{f_S} \quad (22)$$

Expressions (21) and (22) yield the required values of the incident beam parameters for the spherical mirror mode converter to yield a pure  $LG_{01}$  mode. These can in turn be used to calculate the required beam waist size and its distance from the AMC. It is important to note here the calculation for the beam waist size should take into account the mode order and hence the  $M^2$  parameter for the  $HG_{01}^{45}$  beam in orthogonal  $S$  and  $T$  planes. The use of incorrect incident beam parameters will manifest in an error in the Gouy phase difference and an impure final  $LG_{01}$  mode, so care should be taken to provide a suitably tailored input beam. Compared to the cylindrical lens AMC, the spherical mirror AMC has the attractions that fewer components (and optical surfaces) are required leading to lower loss and, hence the potential for use at higher power levels without degradation in mode quality. Moreover, the spherical mirror AMC design is aplanatic and hence can be employed over a broad range of wavelengths.

### III. FIRST-ORDER HERMITE-GAUSSIAN LASER

A prerequisite for generating a high quality  $LG_{01}$  mode via the AMC is a  $HG_{01}$  laser source with high mode purity. In earlier work,  $HG_{01}$  modes have been generated directly in a laser by inserting a thin wire into the resonator to suppress lasing on the Gaussian fundamental ( $HG_{00}$ ) mode [17], [22] or via off-axis laser diode pumping [23], [24]. Both approaches have the shortcoming that they do not provide effective suppression of higher order  $HG_{mn}$

modes leading to significant mode impurity. Moreover, the use of off-axis pumping (or equivalently, mirror misalignment in a  $HG_{00}$  laser) yields an asymmetric temperature profile and consequent beam distortion at high pump powers making power scaling difficult. We have adopted a different approach in which the inversion distribution has been tailored to provide a high spatial overlap with the desired  $HG_{01}$  mode to achieve preferential lasing on this mode. Unwanted modes are suppressed by virtue of having a much poorer overlap with the inversion distribution and hence a higher threshold. This is achieved using an diode-end-pumped Nd:YVO<sub>4</sub> laser configuration with two pump beams adjusted in size and separation to yield an intensity profile in the gain medium that closely resembles that of the  $HG_{01}$  mode.

The experimental set-up for the Nd:YVO<sub>4</sub> laser (shown in Fig. 4) employs a simple two-mirror cavity configuration comprising a plane input coupler with high reflectivity (> 99.8%) at the lasing wavelength (1.064 $\mu$ m) and high transmission (> 95%) at the pump wavelength ( $\sim$  808nm), an antireflection coated 5mm long 1at.% doped Nd:YVO<sub>4</sub> crystal, an antireflection coated plano-convex lens with focal length, 135mm, and a plane output coupler with reflectivity, 95% at the lasing wavelength. The Nd:YVO<sub>4</sub> crystal was mounted in a water-cooled copper heat-sink located immediately adjacent to the input coupler, and the resonator length and lens position were adjusted to yield

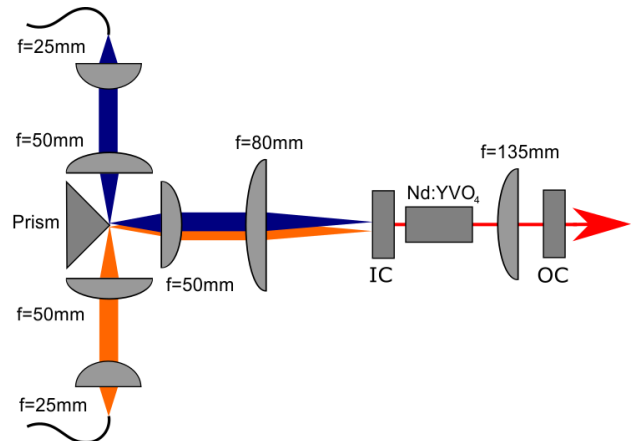


Fig. 4: Schematic of twin-pump-spot diode-end-pumped  $HG_{01}$  Nd:YVO<sub>4</sub> laser.

the desired laser mode size. Pump light was provided by two fiber-coupled diode lasers operating at  $\sim$  808nm. The output from each 105 $\mu$ m diameter (0.22NA) delivery fiber was collimated with a 25mm focal length plano-convex lens and then focussed with the aid of a 50mm focal length plano-convex lens close to the apex of a knife-edge fused silica 45° prism with high reflectivity coatings at 808nm. The two pump beams were aligned in a counter-propagating collinear fashion as shown in Fig. 4 yielding reflected pump beams propagating in the same direction, but with a lateral spacing that could be varied by adjusting the prism position. The beams exiting the prism were then relay imaged by a simple telescope comprising plano convex lenses with focal lengths of 50mm and 80mm into the Nd:YVO<sub>4</sub> crystal. This arrangement yields the desired twin spot pump geometry (shown in Fig. 5(a)) with each

spot having a calculated waist diameter of  $336\mu\text{m}$  in the Nd:YVO<sub>4</sub> crystal with a centre-to-centre spacing of  $538\mu\text{m}$  (i.e. 1.6 times the waist diameter) selected to achieve the optimum overlap with the laser's  $HG_{01}$  mode. Each diode pump could be controlled separately allowing for precisely equal power in each pump spot. Nd:YVO<sub>4</sub> was chosen as the gain medium due to its strongly polarised emission properties, leading to a linearly polarised output without the need of polarization selecting elements, and its short pump absorption length which facilitates mode matching of the pump to the laser mode over the pumped region of the gain medium. The laser resonator was adjusted to give a calculated  $HG_{00}$  mode waist diameter of  $380\mu\text{m}$  on the input coupler (IC), corresponding to calculated  $HG_{01}$  mode sizes of  $658\mu\text{m}$  by  $380\mu\text{m}$  in orthogonal planes. These mode size parameters were optimised experimentally to yield a high quality  $HG_{01}$  output beam (see Fig. 5(b)). The  $HG_{01}$  laser had a threshold pump power of  $224\text{mW}$  and yielded a maximum output power of  $175\text{mW}$  at  $1064\text{nm}$  in a linearly-polarised  $HG_{01}$  beam for a combined incident pump power of  $\sim 1\text{W}$ . The corresponding slope efficiency was 23% and hence somewhat lower than expected. This was attributed to the losses introduced by the intracavity lens and the non-optimum choice of output coupler mirror. At pump powers below  $\sim 1\text{W}$  the laser yielded a high quality  $HG_{01}$  mode output as confirmed by Fig. 5(c), which shows intensity profile through the central portion of the CCD camera image shown in Fig. 5(b) and the numerical fit to a perfect  $HG_{01}$  mode. As pump power was increased beyond  $\sim 1\text{W}$ , the output beam became

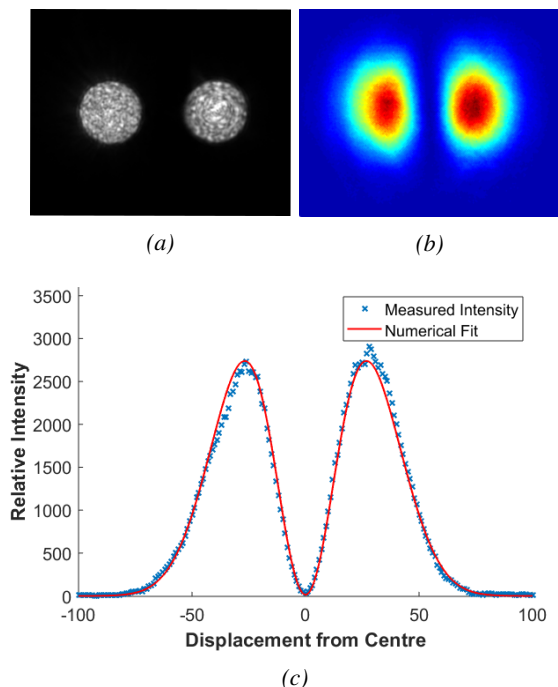


Fig. 5: (a) CCD image of the pump beam at the focus, (b) CCD image of the resulting  $HG_{01}$  laser output, (c) Measured intensity profile through the central section of the laser output beam and numerical fit for a perfect  $HG_{01}$  mode.

degraded due to thermally-induced phase distortion, so, for the purpose of this study, the pump power was limited to below  $\sim 1\text{W}$ . It is worth commenting that the twin-spot end pump architecture adopted here should be applicable to

thin-slab and disk laser geometries to alleviate detrimental thermal effects and allow scaling to considerably higher powers.

#### IV. SPHERICAL MIRROR ASTIGMATIC MODE CONVERTER

The output beam from the Nd:YVO<sub>4</sub> laser was rotated in the  $(x-y)$  plane by  $45^\circ$  with the aid of a dove prism to yield the desired  $HG_{01}^{45}$  input beam for the spherical mirror AMC. The latter (shown in Fig. 6) comprised two high reflectivity  $150\text{mm}$  radius of curvature spherical mirrors aligned at an angle of incidence of  $45^\circ$  for ease of alignment. The mirror spacing was set at  $150\text{mm}$  as stipulated by equation (20) and the input beam was aligned with the aid of two steering mirrors and its size adjusted using a telescope (not shown) to yield a beam incident on

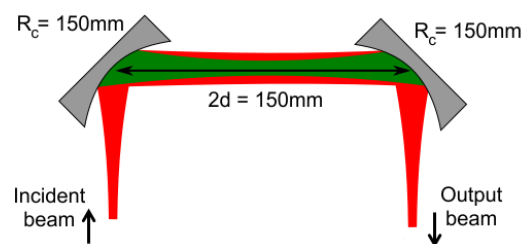


Fig. 6: Schematic of spherical mirror astigmatic mode converter with  $150\text{mm}$  radius of curvature mirrors aligned at  $45^\circ$ .

the first AMC spherical mirror with desired beam radius and wavefront radius of curvature. These conditions were achieved by arranging the incident beam to have a waist radius of  $202\mu\text{m}$  for the  $HG_{01}^{45}$  beam in the  $x$  and  $y$  directions at a position  $96\text{mm}$  away from the first AMC mirror. The  $LG_{01}$  output beam from spherical mirror AMC is shown in Fig. 7(a) and the overall transmission of the AMC was measured to be  $> 99.5\%$ . To confirm the presence of OAM we used the standard method of a Mach-Zehnder interferometer [10], [12], [14]. In this scheme the output

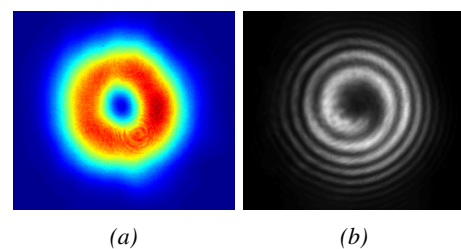


Fig. 7: (a) CCD camera image for the  $LG_{01}^-$  mode output beam at the waist position after the spherical mirror astigmatic mode converter. (b) Spiral interference pattern generated with a Mach-Zehnder interferometer.

beam is collimated and split into two beams; one of which is incident on a pin hole to generate a highly divergent spherical wavefront. The two beams are then re-combined with a beam-splitter to form an interference pattern. If the beam incident on the Mach-Zehnder interferometer is a  $LG_{01}^+$  vortex beam with CW handedness (or an  $LG_{01}^-$  vortex beam with CCW handedness) then the resulting interference pattern is a spiral, where the handedness of the spiral allows differentiation between CW and CCW

handedness. In our experiment, the interference pattern, shown in *Fig. 7(b)*, has a well-defined spiral pattern with CW handedness confirming the presence of a  $LG_{01}^-$  beam. It should be noted that a vortex beam with opposite handedness can be produced by rotating the dove prism before the spherical mirror AMC, so that the input  $HG_{01}$  beam is orientated at  $-45^\circ$  rather than  $+45^\circ$ . While the output beam from the spherical mirror AMC appears, at first sight, to be a very pure  $LG_{01}$  vortex beam, closer inspection of the intensity distribution in *Fig. 7(a)* and the interference pattern in *Fig. 7(b)* reveal that the output beam from the AMC does not have perfect azimuthal symmetry indicating the presence of some mode impurity. Indeed, there are many examples reported in the open literature (see for example [11], [25]) where impurity in generated  $LG_{01}^{+/-}$  modes, evident from a lack in azimuthal uniformity of their intensity profiles, can be severe. This raises the problem of how to quantify the purity of these modes with respect to mode content and calls into question the usefulness of diagnostic techniques such as the observation of spiral interference patterns in a Mach-Zehnder interferometer as a means to evaluate these beams.

## V. VORTEX MODE PURITY

As stated earlier, an  $LG_{01}$  mode can be de-composed into two orthogonal  $HG_{01}$  modes that are  $\pi/2$  out of phase. It therefore follows that any laser cavity capable of supporting an  $LG_{01}$  mode can also support these constituent modes as well. It then follows that these are likely impurities to arise when generating vortex modes via any method internal to a laser cavity. Furthermore, in an AMC, if the input  $HG_{01}$  mode is not perfectly orientated at  $45^\circ$  to the sagittal (or tangential) plane of the AMC, or the AMC is misaligned, then some residual  $HG_{01}$  mode content will remain. We have therefore examined how additional  $HG_{01}$  mode content influences the spiral interference pattern obtained using a Mach-Zehnder interferometer.

The top row of images in *Fig. 8* show the theoretical intensity profiles derived by a coherently combining  $HG_{01}$  and  $HG_{10}$  modes with a  $\pi/2$  phase difference. The first image depicts the scenario where the power levels for  $HG_{01}$  and  $HG_{10}$  modes are equal yielding a perfect  $LG_{01}$  vortex

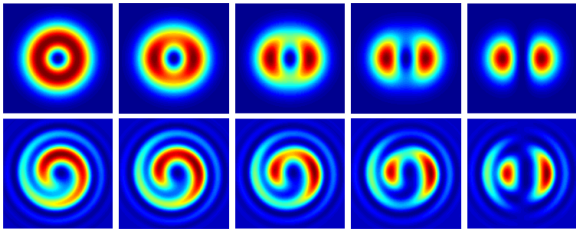


*Fig. 8:* Theoretical intensity profiles generated by coherently combining  $HG_{01}$  and  $HG_{10}$  modes with a  $\pi/2$  phase difference, where the power level in the  $LG_{10}$  for successive images from left to right is 100%, 86%, 66.6%, 40% and 0% respectively of the total beam power (Top row). Corresponding Mach-Zehnder interference patterns (Bottom row).

mode labelled as having 100%  $LG_{01}$  mode content. The second, third, fourth and fifth images show the intensity profiles that result from an increasing imbalance in power in power between the  $HG_{01}$  and  $HG_{10}$  modes such that

the  $LG_{01}$  mode purity decreases to 86%, 66.6%, 40% and 0% of the total power, respectively. This simulation would apply to the scenario where the input beam deviates from  $45^\circ$  by increasing angles, showing that the output beam would evolve from a pure  $LG_{01}$  mode to a pure  $HG_{10}$  mode. The lower set of images in *Fig. 8* show the theoretical interference patterns generated by interfering the beams in the top row with a coherent spherical wave,  $E_{Sph}$ , given by (23):

$$E_{Sph} = \left(\frac{1}{r}\right) \exp(ikr). \quad (23)$$

As expected, the interference pattern for the pure  $LG_{01}$  mode has a clear spiral shape and this degrades as the imbalance in power between the constituent  $HG_{01}$  and  $HG_{10}$  increases. However, it is quite striking that the spiral pattern is still very visible even when the power for the  $HG_{10}$  mode is only 40 % of the total power. This simulation clearly shows that the observation of a spiral interference pattern with a Mach-Zehnder interferometer is not a sufficient test for vortex mode purity. The intensity profile for the pure  $LG_{01}$  mode and its interference pattern are azimuthally symmetrical. However, for the scenario depicted in *Fig. 8*, where mode impurity arises from an imbalance in power for the constituent  $HG_{01}$  and  $HG_{10}$  modes, the intensity profile of the resulting output beam and the corresponding interference pattern show increasing azimuthal asymmetry as power imbalance increases. Thus, analysis of the azimuthal intensity variation can yield quantitative information on  $LG_{01}$  mode purity for this common cause of beam distortion. Experimentally, the azimuthal variation in intensity could be measured by, for example, rotating a narrow slit aligned with its axis of rotation at the beam's centre and recording the power variation. *Fig. 9(a)* shows the calculated intensity variation as a function of slit azimuthal angle,  $\theta$ , for the scenarios shown in *Fig. 8*, and *Fig. 9(b)* shows the relative variation in transmitted power versus purity level for the  $LG_{01}$ . This approach for characterising the beam has the attraction that even a relatively low level of mode impurity can be detected. Moreover, this can be used as a diagnostic for optimising the alignment of the spherical mirror AMC to reduce beam asymmetry due to mode distortion. It is important to note, however, that this method will not reveal undesirable Gaussian  $HG_{00}$  mode content as this impurity is azimuthally symmetric. Therefore, its application is limited to systems where  $HG_{01}$  mode impurities are the most likely, such as AMCs.

## VI. MODE CONVERTER PERFORMANCE

To evaluate the performance of the spherical mirror AMC and the impact of misalignment on  $LG_{01}$  mode purity, the dove prism was adjusted to incrementally change the angle of orientation of the incident  $HG_{01}$  mode from its optimum orientation at  $45^\circ$  to approximately  $\sim 1^\circ$ . This allowed us to introduce a known amount of excess  $HG_{01}$  mode impurity. The theoretical impact on  $LG_{01}$  mode purity (i.e. fraction of the power in the desired  $LG_{01}$  mode compared to the total power after the AMC) is plotted in *Fig. 10(a)* as a function of  $HG_{01}$  orientation from  $45^\circ$ . At each angle, the resulting output beam was

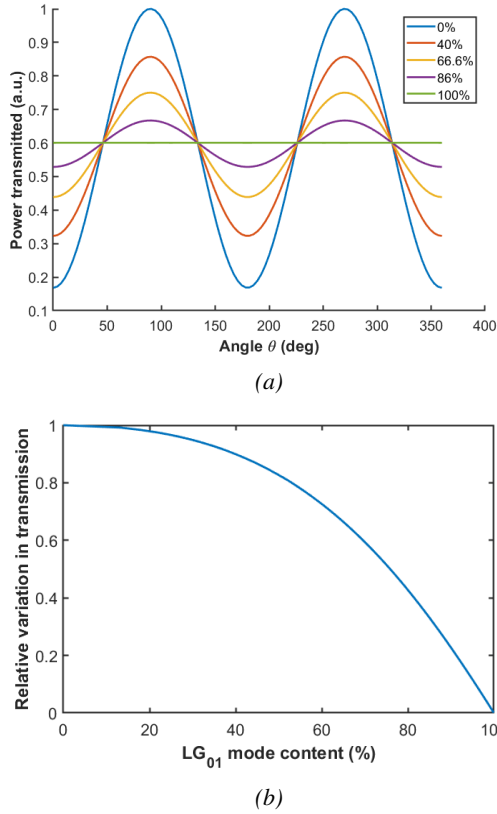


Fig. 9: (a) Calculated intensity variation versus azimuthal angle,  $\theta$ , for the interference patterns in Fig. 8. (b) Relative intensity variation as a function of  $LG_{01}$  mode content.

evaluated by recording the intensity profile, the Mach-Zehnder interference pattern and, with the aid of a slit mounted on a rotation stage, the azimuthal variation in intensity was measured. We can then estimate the  $LG_{01}$  mode content for each  $HG_{01}$  orientation from the theoretical curve in Fig. 10(a). Example converted beam images and Mach-Zehnder interference patterns are shown in Fig. 10(b). The modes depicted correspond to approximately, from left to right, 100%, 88%, 63%, 42% and 3%  $LG_{01}$  content. These experimental results show that the spiral pattern is clearly discernible, if degraded, even when the output beam has only  $\sim 63\%$  of the power in the  $LG_{01}$ . It should be stressed that these are theoretical estimates for the  $LG_{01}$  mode content for a perfectly performing AMC with a perfect  $LG_{01}$  mode input beam, albeit with an angular misalignment from  $45^\circ$ . Once again the experimental results confirm the need for greater scrutiny when assessing mode purity. The variation in measured azimuthal intensity, shown in Fig. 11, can be compared with the theory in Fig. 9(b) to gauge the actual level of  $LG_{01}$  mode purity for different input angles of the  $HG_{01}$  beam. In this case the optimum input angle orientation (i.e.  $\theta = 45^\circ$ ) yields an  $LG_{01}$  mode purity of 94%. This assumes that the main source of mode impurity is an imbalance in the powers for the constituent  $HG_{01}$  and  $HG_{10}$  modes due to imperfect alignment of the incident beam and/or AMC or non-optimum input beam parameters (i.e. beam size and wavefront radius of curvature). This result shows that high purity  $LG_{01}$  vortex beams can be produced by the spherical mirror AMC in combination with a high purity incident

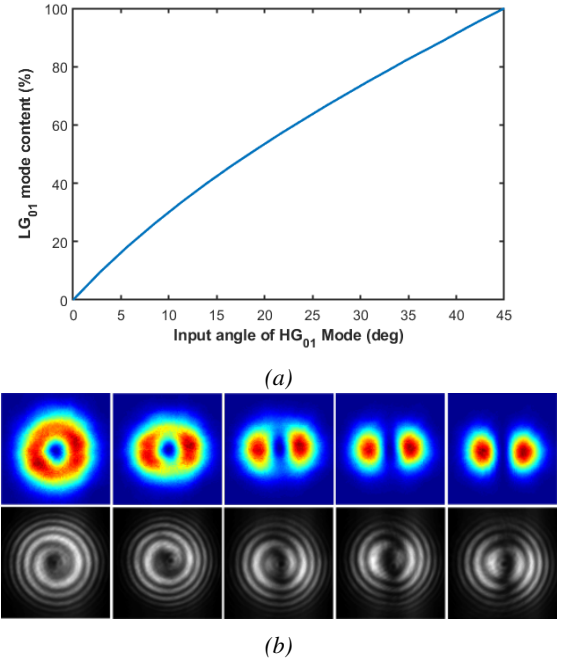


Fig. 10: (a) shows the relation between the input angle of the  $HG_{01}$  mode and the expected percentage of  $LG_{01}^+$  contained in the converted mode. The top row of (b) depicts the  $LG_{01}$  modes converted from input  $HG_{01}$  modes at, from left to right, input angles of  $45^\circ$ ,  $39^\circ$ ,  $25^\circ$ ,  $15^\circ$  and  $1^\circ$ . The bottom row shows their corresponding Mach-Zehnder interference patterns.

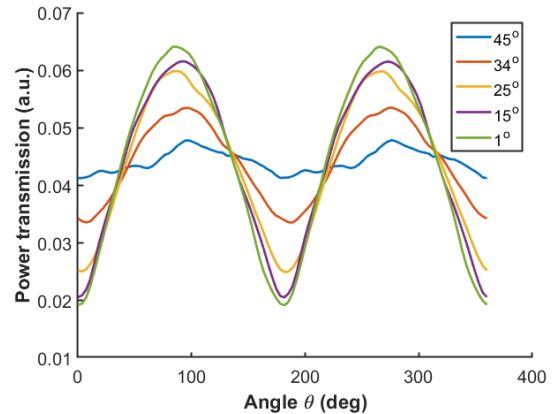


Fig. 11: Azimuthal variation in transmitted intensity for different  $HG_{01}$  mode orientations.

$HG_{01}$  beam. Further improvement in  $LG_{01}$  mode impurity should be possible through careful optimisation of the input beam parameters and AMC alignment to minimise azimuthal variation in intensity.

## VII. CONCLUSIONS

In summary, we have demonstrated an improved method for generating high purity  $LG_{01}$  vortex modes by utilising a novel twin-spot end pumping scheme to directly generate a high quality  $HG_{01}$  mode from a solid-state laser followed by a novel AMC based on spherical mirrors. We have also shown that the standard method for confirming the presence of a vortex mode (i.e. by observation of a spiral interference pattern in a Mach-Zehnder interferometer) does not provide a satisfactory gauge of mode purity and

can yield misleading results. To remedy this short coming we have added an additional diagnostic test to measure the azimuthal intensity variation to identify common causes of vortex mode impurity based on a imbalanced contributions from constituent  $HG_{01}$  and  $HG_{10}$  modes. This approach allows an accurate estimate of vortex mode purity in many situations of practical interest and will prove very useful when assessing the relative merits of different approaches for generating vortex modes. Using this simple diagnostic approach, we have shown that our scheme can yield an  $LG_{01}$  vortex mode with very high purity ( $\sim 94\%$ ) and that further improvement in mode purity may be possible via further optimisation the AMC and input beam parameters. Furthermore, scaling to high power levels, as required by applications such as materials processing, should be readily achievable by combining this scheme with a disk (or slab) gain medium architecture.

#### ACKNOWLEDGMENT

R. Uren and C.R.Smith acknowledge support from the Engineering and Physical Sciences Research Council (EPSRC) for studentships. The data underpinning this publication is available from the University of Southampton repository at <http://doi.org/????>.

#### REFERENCES

- [1] Cyril Hnatovsky, Vladlen G Shvedov, Wieslaw Krolikowski, and Andrei V Rode. Materials processing with a tightly focused femtosecond laser vortex pulse. *Optics letters*, 35(20):3417–9, October 2010.
- [2] Kai Izumisawa, Ablimit Abulizi, Honami Fujiwara, Yuri Nakamura, Tatsuyuki Sugimoto, Katsuhiko Miyamoto, and Takashige Omatsu. Crystalline silicon (111) needle formed by optical vortex illumination. In *2017 Conference on Lasers and Electro-Optics Europe & European Quantum Electronics Conference (CLEO/Europe-EQEC)*, pages 1–1. IEEE, jun 2017.
- [3] Fuyuto Takahashi, Katsuhiko Miyamoto, Hirofumi Hidai, Keisaku Yamane, Ryuji Morita, and Takashige Omatsu. Picosecond optical vortex pulse illumination forms a monocrystalline silicon needle. *Scientific Reports*, 6(1):21738, April 2016.
- [4] Junichi Hamazaki, Ryuji Morita, Keisuke Chujo, Yusuke Kobayashi, Satoshi Tanda, and Takashige Omatsu. Optical-vortex laser ablation. *Opt. Express*, 18(3):2144–2151, Feb 2010.
- [5] Marti Duocastella and Craig B Arnold. LASER & PHOTONICS REVIEWS Bessel and annular beams for materials processing. *Laser Photonics Rev*, 6(5):607–621, 2012.
- [6] Igor A Litvin, Sandile Ngcobo, Darry Naidoo, Kamel Ait-Ameur, and Andrew Forbes. Doughnut laser beam as an incoherent superposition of two petal beams. *Optics letters*, 39(3):704–7, February 2014.
- [7] Tom Dietrich, Martin Rumpel, Thomas Graf, and Marwan Abdou Ahmed. Efficient generation of cylindrically polarized beams in an Yb:YAG thin-disk laser enabled by a ring-shaped pumping distribution. volume 9893, page 98930M. International Society for Optics and Photonics, April 2016.
- [8] J. W. Kim, J. I. Mackenzie, J. R. Hayes, and W. A. Clarkson. High power Er:YAG laser with radially-polarized Laguerre-Gaussian (LG<sub>01</sub>) mode output. *Optics Express*, 19(15):14526, July 2011.
- [9] J.W. Kim and W.A. Clarkson. Selective generation of LaguerreGaussian (LG<sub>0n</sub>) mode output in a diode-laser pumped Nd:YAG laser. *Optics Communications*, 296:109–112, June 2013.
- [10] Yongguang Zhao, Qiyao Liu, Wei Zhou, and Deyuan Shen.  $\sim 1$  mJ pulsed vortex laser at 1645 nm with well-defined helicity. *Optics Express*, 24(14):15596, July 2016.
- [11] Shiwen Tan, Changhe Zhou, Akira Shirakawa, Kenichi Ueda, and Jianlang Li. Vortex Ti:Sapphire laser by using an intracavity spot-defect spatial filter. *Optics & Laser Technology*, 96:76–80, November 2017.
- [12] Di Lin, J M O Daniel, and W A Clarkson. Controlling the handedness of directly excited Laguerre-Gaussian modes in a solid-state laser. *Optics letters*, 39(13):3903–6, July 2014.
- [13] M.W. Beijersbergen, R.P.C. Coerwinkel, M. Kristensen, and J.P. Woerdman. Helical-wavefront laser beams produced with a spiral phaseplate. *Optics Communications*, 112(5-6):321–327, dec 1994.
- [14] K Sueda, G Miyaji, N Miyana, and M Nakatsuka. Laguerre-Gaussian beam generated with a multilevel spiral phase plate for high intensity laser pulses. *Optics Express*, 12(15):3548–3553, 2004.
- [15] A. Jesacher, A. Schwaighofer, S. Frhapter, C. Maurer, S. Bernet, and M. Ritsch-Martel. Wavefront correction of spatial light modulators using an optical vortex image. *Optics Express*, 15(9):5801–5808, 2007.
- [16] Chr. Tamm and C. O. Weiss. Bistability and optical switching of spatial patterns in a laser. *J. Opt. Soc. Am. B*, 7(6):1034–1038, Jun 1990.
- [17] M.W. Beijersbergen, L. Allen, H.E.L.O. van der Veen, and J.P. Woerdman. Astigmatic laser mode converters and transfer of orbital angular momentum. *Optics Communications*, 96(1-3):123–132, February 1993.
- [18] J. Courtial and M.J. Padgett. Performance of a cylindrical lens mode converter for producing LaguerreGaussian laser modes. *Optics Communications*, 159(1):13–18, 1999.
- [19] Robert W. Boyd. Intuitive explanation of the phase anomaly of focused light beams. *Journal of the Optical Society of America*, 70(7):877, July 1980.
- [20] H. Kogelnik and T. Li. Laser Beams and Rsonators. *Applied Optics*, 5(10):1550–1567, 1966.
- [21] A.E. Siegman. *Lasers*. University Science Books, 1986.
- [22] A A Malyutin and V A Ilyukhin. Generation of high-order hermitegaussian modes in a flashlamp-pumped neodymium phosphate glass laser and their conversion to laguerregaussian modes. *Quantum Electronics*, 37(2):181, 2007.
- [23] Takayuki Ohtomo, Shu-Chun Chu, and Kenju Otsuka. Generation of vortex beams from lasers with controlled Hermite- and Ince-Gaussian modes. *Optics Express*, 16(7):5082, March 2008.
- [24] Shu-Chun Chu and Kenju Otsuka. Doughnut-like beam generation of LaguerreGaussian mode with



extremely high mode purity. *Optics Communications*, 281(6):1647–1653, March 2008.

- [25] Qiyao Liu, Bin Zhang, Sisheng Qi, Yaocheng Li, Xuliang Fan, Yongguang Zhao, Wei Zhou, and Deyuan Shen. Integration of helicity-control and pulse-modulation for vortex laser based on a black phosphorus plate. *Optics Express*, 2016.